Composites Communications 22 (2020) 100519

Contents lists available at ScienceDirect

Composites Communications

journal homepage: www.elsevier.com/locate/coco

Highly porous electroactive polyimide-based nanofibrous composite anode for all-organic aqueous ammonium dual-ion batteries

Gangyong Zhou [a], Xingyu An [a], Chunyang Zhou [a], Yue Wu [c], Yue-E Miao [a,*], Tianxi Liu [a,b,**]

[a] State Key Laboratory for Modification of Chemical Fibers and Polymer Materials, College of Materials Science and Engineering, College of Mechanical Engineering, Donghua University, Shanghai, 201620, PR China

[b] Key Laboratory of Synthetic and Biological Colloids, Ministry of Education, School of Chemical and Material Engineering, Jiangnan University, Wuxi, 214122, PR China

[c] Research Center for Analysis and Measurement, Donghua University, Shanghai, 201620, PR China

ARTICLE INFO

Keywords:
Electroactive polyimide
Composite nanofiber
Highly porous structure
Aqueous ammonium dual-ion batteries

ABSTRACT

Aqueous ammonium dual-ion batteries (ADIBs), especially those integrating organic electroactive materials and functioning in a mild electrolyte of ammonium sulfate solution, have attracted increasing attentions in the stationary electrochemical storage area due to their inherent safety, sustainability, and environmental friendliness features. Herein, a flexible electroactive polyimide/nitrogen-doped carbon/carbon nanotubes (PI/NDC/CNT) composite nanofiber membrane with highly interconnected conductive porous structure is prepared through electrospinning and in-situ pyrolysis/imidization treatments for ADIB applications. The electroactive PI achieves uniform distribution, high utilization and ultrafast reaction kinetics within PI/NDC/CNT electrode. As a result, the PI/NDC/CNT electrode exhibits high reversible capacity of 161 mA h g^{-1} at 0.5 A g^{-1}, good rate capability, and satisfying capacity retention over 87.9% after 5000 cycles. Besides, an all-organic aqueous ADIB using PI/NDC/CNT and polyaniline/carbon nanofiber composites as anode and cathode respectively, achieves ultralong cycle stability and high energy density of 114.3 W h kg^{-1}.

1. Introduction

Currently, the development of safe, sustainable and environmentally friendly energy storage devices for large-scale applications is considered to be one of the top priorities due to the ever-growing energy and environmental crises [1–11]. Aqueous rechargeable batteries show great potentials because of their inherent safety, fast kinetics and environmental friendliness compared to their non-aqueous counterparts [7,12–17]. Up to now, numerous aqueous "rocking-chair" batteries have been reported based on Li^+ [13,18,19], Na^+ [11,15,20], K^+ [16,21], Zn^{2+} [22–24] and Al^{3+} [7,25]. Nevertheless, the narrow working potential window of water caused by the evolution reactions of H_2 or O_2 and the enlarged ionic radius of hydrated ions lead to the low energy density and poor cycle life of aqueous rechargeable batteries. To meet the commercial requirements of high working voltage, high energy density and environmental friendliness, aqueous rechargeable dual-ion batteries [26–31], with both cations and anions simultaneously participating in the intercalation/deintercalation of anodes and cathodes, are one of the most promising candidates. Unfortunately, the traditional metal-based inorganic electrode materials deliver inferior rate performance and poor cyclability in the aqueous dual-ion batteries because of their intrinsically poor conductivity and severe volume expansion during discharge/charge processes. In contrast, organic aqueous ammonium dual-ion batteries (ADIBs) [26,32,33], which employ organic electroactive materials as electrode materials and ammonium ion (NH_4^+) as the charge carrier, are considered as ideal battery systems due to the abundant sources, small hydrated ionic size (3.31 Å) and low molar mass (18 g mol^{-1}) of NH_4^+ compared with metal ions such as Na^+, K^+, Zn^{2+}, Mg^{2+} and Al^{3+}. Therefore, novel organic aqueous ADIBs are expected as promising candidates for large-scale applications.

As a new-rising organic aqueous battery system, the choice of electrode materials essentially defines the properties of ADIBs. Especially, the electroactive organic compounds have been demonstrated as a

* Corresponding author.
** Corresponding author. State Key Laboratory for Modification of Chemical Fibers and Polymer Materials, College of Materials Science and Engineering, College of Mechanical Engineering, Donghua University, Shanghai, 201620, PR China.
E-mail addresses: yuee_miao@dhu.edu.cn (Y.-E. Miao), txliu@dhu.edu.cn (T. Liu).

https://doi.org/10.1016/j.coco.2020.100519
Received 15 September 2020; Received in revised form 24 September 2020; Accepted 24 September 2020
Available online 4 October 2020

favorable substitution for transition metal-based electrode materials due to their advantages of low cost, good tolerance of ionic size and environmental friendliness [32,34–36]. More importantly, the designable molecular structures of organic compounds can guarantee the tuning of their flexibility and solubility, electrochemical stability and reversibility, as well as redox potentials, thereby optimizing the cell voltage without triggering severe O_2 or H_2 evolutions [34,35,37]. Generally, these electroactive organic compounds can be classified into n-type and p-type compounds based on their doping types [26,37]. As for n-type compounds, the reversible reactions carry out between the neutral state and negatively charged state, where cations are needed to neutralize the negative charge of n-type compounds. Correspondingly, in p-type compounds, the reversible reactions happen between the neutral state and positively charged state by incorporation of anions, thus resulting in higher redox potentials than those of n-type compounds. Therefore, the regulation of different redox potentials between p-type and n-type compounds can construct high operating voltage and energy density of aqueous ADIBs. To date, several types of electroactive organic compounds have been reported for constructing ADIB electrodes, such as quinone [35], Prussian blue [38,39], polyimide [26], polynorbornenes [34], polyaniline [32] and radical polymers [33]. Among them, polyimide, as a typical n-type compound, has been widely investigated as anode materials for aqueous ADIBs due to its plenty of electroactive functional groups (C═O), tunable redox potentials and stable structure during the discharge/charge processes. However, the electrochemical performance of polyimide is still limited in aqueous ADIBs because of the unsatisfactory electrical conductivity, agglomeration of powdery structure and polymer binder usage, which induces sluggish reaction kinetics and limited utilization of the electroactive functional groups. Therefore, it is urgent but challenging to develop polyimide-based electrode material with superior conductivity, efficient utilization of electroactive functional groups and ultrafast reaction kinetics for aqueous ADIBs.

Combination of conductive carbon nanomaterials and porous structural design is an efficient method to realize the excellent electrochemical performance of polyimide-based electrode materials in aqueous ADIBs. As a promising conductive carbon nanomaterial, carbon nanotubes (CNT) can not only provide conducting network structure for electron transfer, but also enable excellent mechanical property because of its high tensile strength. However, the agglomeration of CNT leads to deteriorated electrical conductivity and specific capacity, and sluggish reaction kinetics of the electrodes in practical applications. To address these issues, we report a highly porous electroactive polyimide composite nanofiber electrode in this work for aqueous ADIB applications. Consisting of electroactive polyimide (PI) derived from the polycondensation of 1,4,5,8-naphthalenetetracarboxylic dianhydride (NTCDA) and *p*-phenylenediamine (PDA), nitrogen-doped carbon (NDC) and carbon nanotubes (CNT), the highly porous nanofibrous PI/NDC/CNT composite electrode via in-situ pyrolysis and imidization can effectively prevent the agglomeration of PI and CNT, as well as present enhanced conductivity. Hence, rapid ionic/electronic transport is achieved within the highly porous conductive structure, largely boosting the electrochemical energy storage efficiency. As a result, the PI/NDC/CNT electrode exhibits high reversible capacity of 161 mA h g^{-1} at 0.5 A g^{-1}, good rate capability, and satisfying capacity retention over 87.9% after 5000 cycles. Furthermore, based on the reaction mechanisms of n-type and p-type compounds respectively, a green organic aqueous ADIB is reasonably assembled employing the PI/NDC/CNT anode and polyaniline/carbon nanofiber (PANI/CNF) composite cathode as illustrated in Fig. 1. The aqueous PI/NDC/CNT//PANI/CNF ADIB delivers wide operating voltage of 1.9 V, and high energy density of 114.3 W h kg^{-1} at the power density of 18.6 kW kg^{-1} in a mild aqueous ammonium sulfate solution. Therefore, the reasonable construction of PI/NDC/CNT composite electrode in this work can provide new ideas and references for developing sustainable and advanced ADIBs.

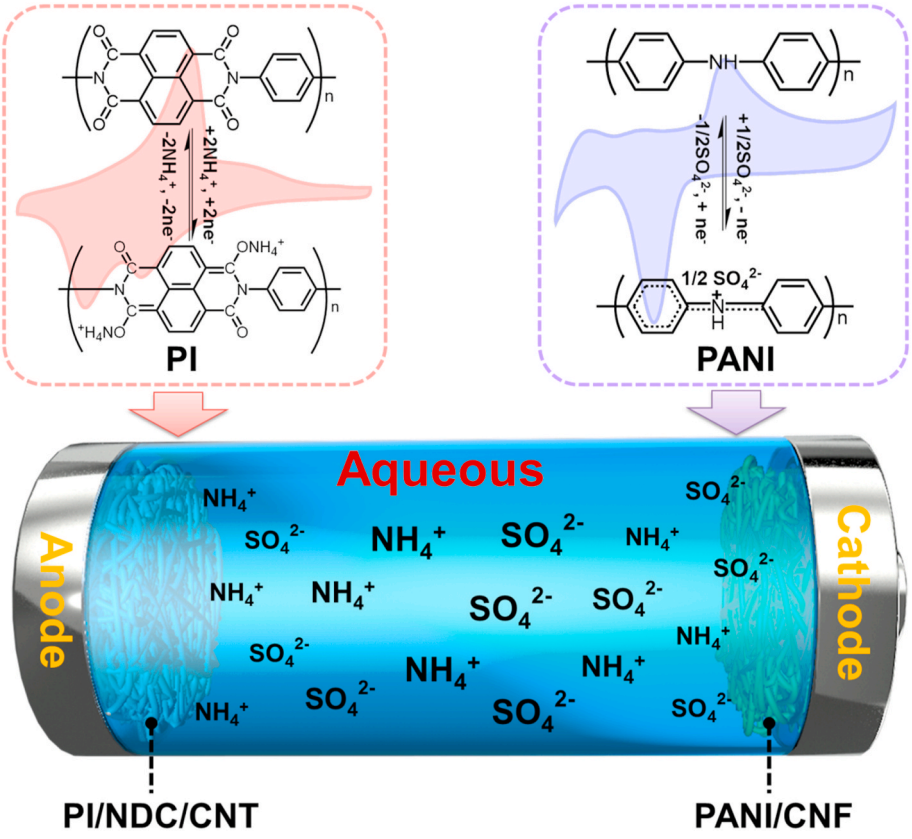

Fig. 1. Schematic of the all-organic aqueous ADIB assembled with PI/NDC/CNT anode and PANI/CNF cathode, respectively.

2. Experimental

2.1. Materials

All materials were used as received. 1,4,5,8-naphthalenetetracarboxylic dianhydride (NTCDA, AR) and *p*-phenylenediamine (PDA, AR) were purchased from TCI, Tokyo Chemical Industry Co., Ltd, Tokyo, Japan. Polyacrylonitrile (PAN, M_w = 86,000), polymethyl methacrylate (PMMA, M_w = 350,000), *N,N*-dimethylformamide (DMF, 99.9%), concentrated sulfuric acid (H_2SO_4, 96–98%), ammonium persulfate (APS, AR), aniline monomers (AN, AR) and ammonium sulfate ($(NH_4)_2SO_4$, AR) were purchased from Sigma-Aldrich. Multi-walled carbon nanotubes (MWCNT, 10–20 nm in diameter and 10–30 μm in length) were supplied by Chengdu Institute of Organic Chemistry, Chinese Academy of Sciences, China. The carbon cloth was provided by Shanghai Hesen Corporation, China. Deionized (DI) water was used throughout the experiments.

2.2. Synthesis of PI/NDC/CNT composite nanofiber membrane

The CNT dispersion solution was obtained using acid treatment according to previous report [40]. Equal molar amounts of NTCDA (0.005 mol) and PDA (0.005 mol) were mixed in 20.0 g of DMF in a 100 mL round-bottom flask equipped with a mechanical stirrer, and then intensely stirred at 120 °C for 12 h under Ar atmosphere. A viscous polymer solution was obtained after polycondensation, which was signed as PAA. After that, the PAA/PAN/PMMA/CNT dispersion solution was obtained by dissolving 5.0 g of PAA solution, 0.7 g of PMMA, 0.17 g of PAN and 5.0 g of the treated CNT dispersion solution under Ar atmosphere. The PAA/PAN/PMMA/CNT dispersion solution was electrospun into nanofiber membrane by applying an electrical potential of 15 kV, and then dried at 80 °C in a vacuum oven and heat-treated at 400 °C under Ar for another 2 h to obtain the PI/NDC/CNT composite nanofiber membrane.

2.3. Synthesis of CNF and PANI/CNF nanofiber membranes

The flexible carbon nanofiber membrane was prepared as previously reported [41]. Briefly, PAN nanofiber membrane was obtained by electrospinning at a concentration of 10 wt%. Then, it was pre-oxidized under air atmosphere at a heating rating of 1 °C min^{-1} to 230 °C and maintained for 3 h, and then carbonized under Ar atmosphere with a heating rate of 5 °C min^{-1} to 1000 °C and maintained for 2 h, thus resulting in the flexible CNF membrane with excellent electrical and mechanical properties. After that, *in situ* oxidative polymerization of aniline was carried out on the surface of CNF using APS as an oxidizing agent to obtain the flexible PANI/CNF composite membrane. Typically, the flexible CNF membrane was immersed in 50 mL of 1.0 M H_2SO_4 solution containing 5.0 mmol of AN at 0 ± 2 °C. Then, 50 mL of 1.0 M H_2SO_4 solution dissolving with APS was added dropwise into the above solution at an APS/AN mole ratio of 1/4 to obtain the reaction solution and keep stirring for another 6 h at 0 ± 2 °C. Finally, the flexible PANI/CNF composite membrane was washed with DI water, and dried under vacuum at 60 °C for 12 h. The loading amount of PANI in the flexible PANI/CNF membrane was calculated based on the mass difference of the dried samples before and after polymerization.

2.4. Characterizations

The chemical structures and compositions of the samples were characterized by Fourier transform infrared (FTIR, NicoletIn10MX/Nicolet 6700, Thermo Fisher, USA), ^{13}C nuclear magnetic resonance (^{13}C NMR, BrukerAvance 400, Switzerland), and thermogravimetric analyzer (TGA, NETZSCH TG 209 F1 Libra®, Germany) with a temperature ramp of 10 °C min^{-1} under Ar atmosphere, respectively. Morphologies of PAA/PAN/PMMA/CNT, PI/NDC/CNT and PANI/CNF nanofiber membranes were observed using field-emission scanning electron microscope (FESEM, HitachiS-8010, Japan) and transmission electron microscope (TEM, Talos F200S, Thermo Fisher, USA).

2.5. Electrochemical tests

For a three-electrode measurement, the PI/NDC/CNT nanofiber membrane was directly used as a binder-free working electrode, while the carbon cloth and a saturated calomel electrode (SCE) were used as the counter and reference electrodes, respectively. An aqueous solution of 1.0 M $(NH_4)_2SO_4$ was used as the electrolyte. The aqueous ADIBs were fabricated in a CR2032 coin-type cell, where PI/NDC/CNT and PANI/CNF nanofiber membranes were directly used as the binder-free anode and cathode respectively and the cellulose film served as the separator. The galvanostatic charge-discharge (GCD) tests were conducted on a battery-testing system (Land CT-2001A, Wuhan, China). Cyclic voltammetry (CV) and electrochemical impedance spectroscopy (EIS, 0.01 Hz-100 kHz, 5 mV) measurements were performed on an electrochemical workstation (CHI 760D, China).

3. Results and discussion

The FTIR and ^{13}C NMR spectra were obtained to confirm the compositions of different samples. As shown in Fig. 2a, the PI/NDC/CNT composite shows obvious characteristic vibration absorption peaks of imide C═O and C–N bonds at 1717 cm^{-1}, 1673 cm^{-1} and 1347 cm^{-1} respectively, while the NDC/CNT composite shows indistinct broad absorption peaks in the FTIR spectrum. Additionally, the ^{13}C NMR spectrum of PI/NDC/CNT in Fig. 2b indicates the conjugated carbonyl groups from imide rings of PI at 162 ppm and aromatic carbon of phenyl or naphthalene in the range of 125–147.5 ppm [42], respectively, fully confirm the formation of PI in the composite nanofibers. As analyzed by TGA in Fig. 2c, CNT maintains stable at 400 °C while in-situ decompositions of PAN, PMMA, PAA take place to construct porous structures. The exact loading amount of PI in PI/NDC/CNT composite is calculated to be 60% according to the different weight losses of PAN, PMMA, PAA and PAA/PAN/PMMA/CNT after heat-treated at 400 °C. The surface morphology of PI/NDC/CNT (Fig. 2d) indicates a three-dimensional (3D) interwoven network structure with uniform fiber diameter. In addition, carbon nanotubes are evenly dispersed within the single porous nanofiber (Fig. 2e). The high-magnification cross-sectional SEM (Fig. 2f) and TEM (Fig. 2g) images, and energy dispersive spectroscopy (EDS) mappings (Fig. 2h) further reveal that the different compositions are homogenously distributed in the interconnected fibrous structure. Hence, high conductivity and superior wettability toward electrolytes are achieved, which greatly enhances the electron and ion transport inside PI/NDC/CNT composite electrode during the electrochemical cycles.

The electrochemical properties of the as-obtained PI/NDC/CNT composite electrode were characterized by CV, GCD and EIS tests in a three-electrode system with 1.0 M $(NH_4)_2SO_4$ aqueous solution. As shown in Fig. 3a, the PI/NDC/CNT electrode shows a pair of broad redox peaks with small potential separations, representing a two-electron transfer reaction with rapid redox reaction kinetics. Moreover, the subsequent CV cycles show stable redox peaks with highly overlapped profiles, indicating an excellent stability of PI/NDC/CNT during cycling. The GCD profiles of PI/NDC/CNT electrode in Fig. 3b exhibit broad voltage plateau in the first five cycles at 0.5 A g^{-1} with a high initial specific capacity of 161 mA h g^{-1}, which are in good consistence with the CV results. The reversible redox peaks indicate that PI can reversibly associate/dissociate with NH_4^+ in the redox processes as shown in Fig. 3c. During discharge, two NH_4^+ associate with the conjugated C═O groups of PI to form ammonium enol compound. Vice versa, the NH_4^+ can reversibly disassociate from the ammonium enol compound [33]. Therefore, the PI/NDC/CNT electrode also shows satisfactory rate capability with high reversible capacities of 160.7, 146.1, 133.2, 123.2,

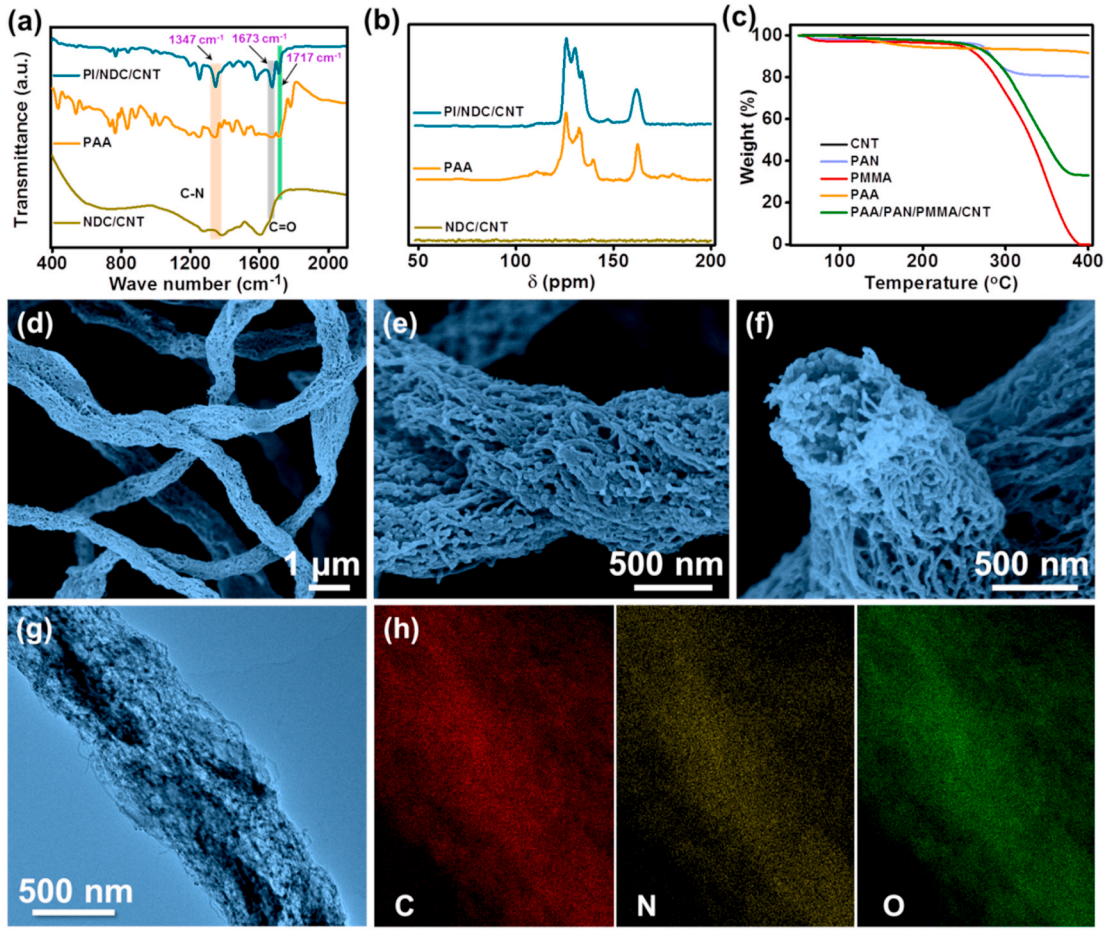

Fig. 2. (a) FTIR, (b) ^{13}C NMR, and (c) TGA curves of different samples. (d–f) SEM, (g) TEM, and (h) the corresponding elemental mappings of the PI/NDC/CNT composite nanofiber membrane.

96.5 mA h g^{-1} at 0.5, 1.0, 2.0, 5.0 and 10.0 A g^{-1}, respectively (Fig. 3d and S1). Besides, an ultra-stable reversible capacity of 121.0 mA h g^{-1} is retained with an average Coulombic efficiency approaching 100% even after 5000 cycles at a high current density of 5.0 A g^{-1} (Fig. 3e). Additionally, the Nyquist plot shows a small semicircle at high frequency and a sloping line at the low frequency region (Fig. S1b), which can be attributed to the low charge-transfer impedance and small Warburg coefficient of the PI/NDC/CNT anode as displayed in Fig. S1c.

In order to investigate the reaction kinetics of the PI/NDC/CNT electrode, CV measurements were performed at various scan rates from 1.0 to 5.0 mV s^{-1}. As displayed in Fig. 4a, the CV curves of PI/NDC/CNT maintain similar shapes with the increase of scan rates, indicating excellent stability and fast reaction kinetics. Additionally, the corresponding redox peak current (i_p) is proportional to the square root of the scan rate ($v^{0.5}$) according to the CV curves at various scan rates (Fig. 4b). Thus, a much higher diffusion coefficient of 2.93 × 10^{-8} cm^2 s^{-1} is obtained for PI/NDC/CNT compared with previous reports [39,43], according to the Randles-Sevcik equation $i_p = 2.69 \times 10^5 CSD^{1/2} v^{1/2} n^{3/2}$, where i_p is the peak current (A), C is the concentration of electrolyte, S is the surface area of the electrode, D is the diffusion coefficient of NH_4^+ (cm^2 s^{-1}), v is the potential scan rate (V s^{-1}), and n is the number of transferred electrons. The reaction kinetics of PI/NDC/CNT electrode is further estimated according to the relationship between log (i_p) and log (v), which can be expressed by the formula $\log(i) = b \times \log(v) + \log(a)$, where i_p and v are the peak current and scan rate respectively while a and b are the tunable parameters. As shown in Fig. 4c, according to the linear relationship between log(i) *versus* log(v) plots, the b values of the redox peaks are calculated as 0.82 and 0.89, respectively. According to the power-law relationship [1], the b value approaches 0.5 in a diffusion-controlled process, while the b value of 1 represents a surface capacitance-dominated process. Therefore, we can speculate that the capacity of PI/NDC/CNT is contributed by both diffusion-controlled and capacitive processes. The contribution ratios are further calculated according to the equation $i(v) = k_1 v + k_2 v^{1/2}$, where $k_1 v$ and $k_2 v^{1/2}$ represent the capacitive-controlled and diffusion-limited currents at a particular voltage, respectively. Both the parameters of k_1 and k_2 are determined from the linear relationship of $i(v)/v^{1/2}$ and $v^{1/2}$ based on equation $i(v)/v^{1/2} = k_1 v^{1/2} + k_2$. Consequently, the contribution ratios of the capacitive processes at different scan rates are in the range of 64.1–91.5% as shown in Fig. 4d. A high proportion of the surface capacitance contributes to excellent rate capability, which can be ascribed to the homogenous distribution of electroactive PI within the nanofiber network and fast reaction kinetics throughout the highly interconnected conductive porous structure.

The p-type polymer is often considered as a promising cathode material for aqueous batteries due to its high redox potentials by incorporation of anions [32,33]. As a typical p-type compound, polyaniline (PANI) can associate/disassociate with anions reversibly and maintain the stable molecular structure during discharge/charge processes [32]. Hence, the flexible PANI/CNF composite membrane was directly used as the cathode for ADIBs. The typical SEM images of CNF (Fig. S2) and PANI/CNF (Fig. 5a) show that CNF nanofiber membrane forms a 3D interwoven network structure with uniform nanofiber diameter at about 200 nm, while a dense layer of PANI nanowires are uniformly covered on the surface of CNF after in-situ polymerization. Besides, the high-magnification SEM (Fig. 5b) and TEM images (Fig. S3) clearly

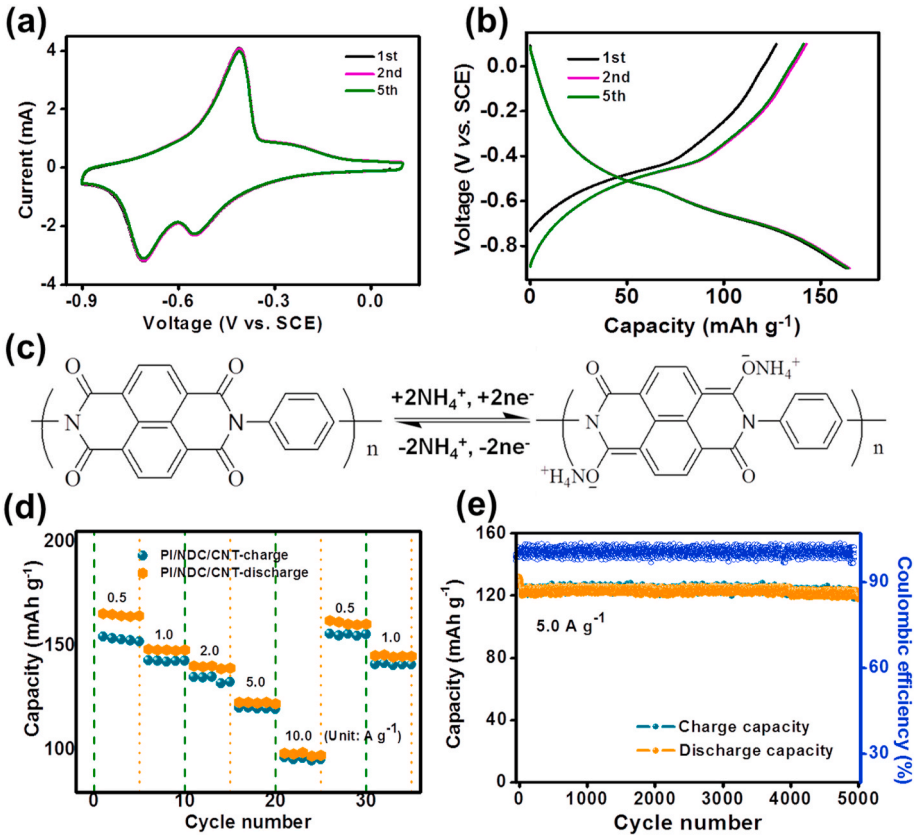

Fig. 3. Electrochemical performances of the PI/NDC/CNT anode in the aqueous ammonium battery: (a) CV curves at a scan rate of 1.0 mV s^{-1}, (b) charge/discharge voltage profiles at a current density of 0.5 A g^{-1}, (c) possible redox mechanisms between PI and NH_4^+, (d) rate performance, and (e) cycling stability at a current density of 5.0 A g^{-1}.

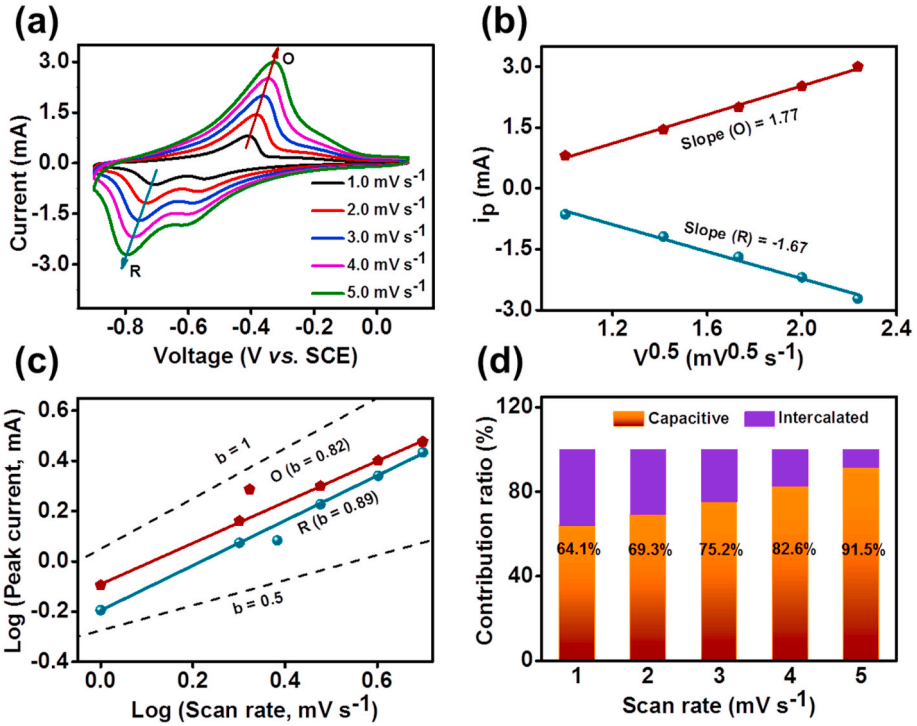

Fig. 4. Electrochemical mechanisms of the PI/NDC/CNT anode in the aqueous ammonium battery: (a) CV curves, (b) linear relationship between the peak current (i_p) and the square root of scan rates ($\nu^{1/2}$), (c) *b*-values analysis, and (d) normalized contribution ratios at different scan rates.

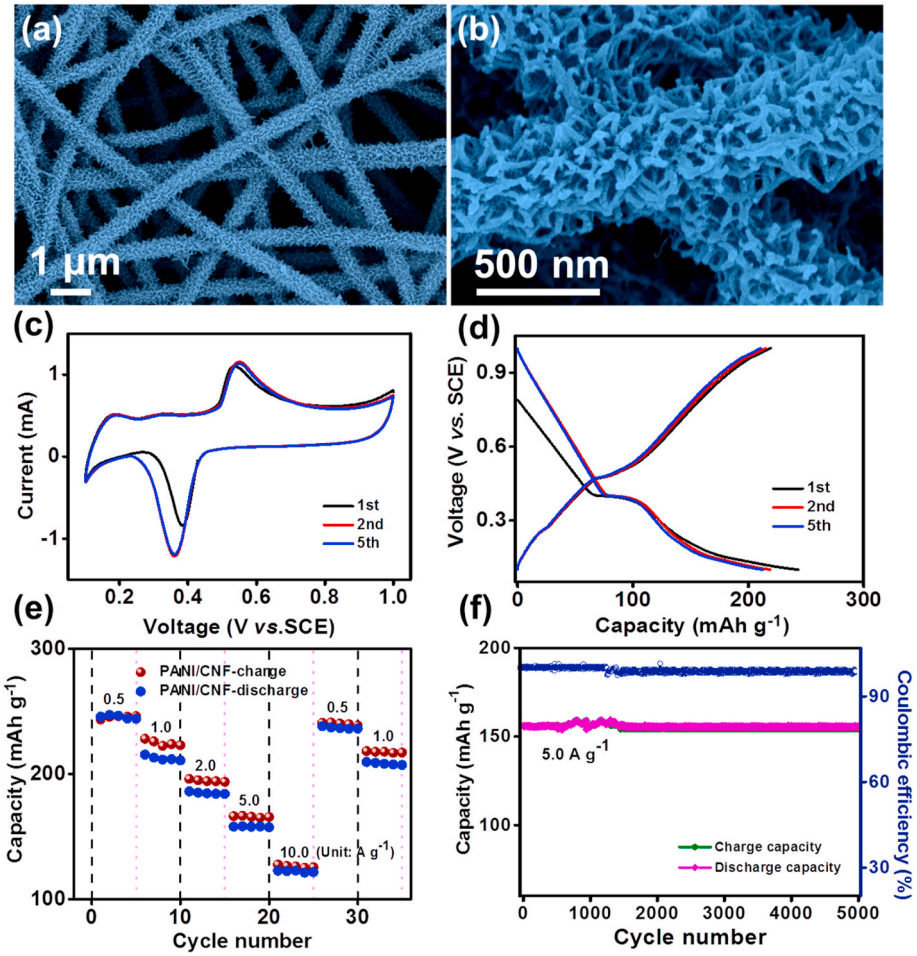

Fig. 5. SEM images of the PANI/CNF composite under different magnifications: (a) Low, and (b) high. (c) CV curves at a scan rate of 1.0 mV s^{-1}, (d) charge/discharge voltage profiles at a current density of 0.5 A g^{-1}, (e) rate performance and (f) cycling stability at a current density of 5.0 A g^{-1} of the PANI/CNF cathode in the aqueous ammonium battery.

reveal that PANI nanowires are connected with each other to construct a hierarchical porous architecture, which is expected to largely enhance the electrochemical performances of the PANI/CNF composite cathode. As shown in Fig. 5c, all the CV curves of PANI/CNF cathode display one couple of symmetrical redox peaks and highly overlapped profiles, indicating an excellent stability of PANI/CNF during cycling. Furthermore, the GCD curves of PANI/CNF cathode also clearly show discharge plateaus, which is well in consistent with the CV results. Meanwhile, a discharge capacity of 212.5 mA h g^{-1} can be obtained at 0.5 A g^{-1} for the PANI/CNF cathode (Fig. 5d) and remains at 122.1 mA h g^{-1} even at a high current density of 10.0 A g^{-1} (Fig. 5e). Furthermore, the PANI/CNF cathode also keeps a very stable discharge capacity of 153.3 mA h g^{-1} after 5000 cycles at 5.0 A g^{-1} (Fig. 5f), demonstrating its superior rate capability and cycle life.

According to the reaction mechanisms of n-type and p-type compounds, an aqueous ADIB is reasonably assembled by respectively using PI/NDC/CNT and PANI/CNF as the anode and cathode at a mass ratio of 2.3 : 1 according to their charge capacities. As shown in Fig. 6a, the PI/NDC/CNT and PANI/CNF composites electrodes effectively work in opposite potential directions. Thus, the NH_4^+ and SO_4^{2-} in the electrolyte will separately move to the anode and cathode during charging. On the contrary, the NH_4^+ and SO_4^{2-} can reversibly break away from the electrode materials and return to the electrolyte, thereby leading to a maximum cell voltage of 1.9 V. Consequently, the CV curve of the aqueous PI/NDC/CNT//PANI/CNF ADIB displays obvious redox peaks at 1.1 V and 1.3 V without polarization phenomenon (Fig. S4a), further confirming a reasonable cell voltage range. As exhibited in Fig. 6b, the aqueous PI/NDC/CNT//PANI/CNF ADIB delivers high discharge capacity of 136.7 mA h g^{-1} and excellent rate capability (Fig. 6c and Fig. S4b). More importantly, a high specific energy density of 114.3 W h kg^{-1} at the high power density of 18.6 kW kg^{-1} is achieved, which is much superior compared with those previously reported aqueous batteries (Fig. 6d). The cycling stability of the as-fabricated ADIB was tested at a current density of 1.0 A g^{-1}. Remarkably, a high reversible capacity of 86.0 mA h g^{-1} is remained after 2000 cycles with an average Coulombic efficiency approaching 100% as shown in Fig. 6e. This is mainly because of the interconnected conductive porous structure and low solubility of electrode materials in the aqueous electrolytes.

4. Conclusions

In summary, the highly porous electroactive polyimide-based composite nanofibrous membrane with well interconnected conductive network structures has been realized for applying as a high-performance organic anode in aqueous ADIBs. The PI/NDC/CNT anode delivers high reversible capacity, excellent rate performance and ultra-long cyclic stability because of the 3D interwoven nanofiber network structure and interconnected conductive porous skeleton, which enables ultrafast ion diffusion and electron transfer during discharge/charge processes. Therefore, highly efficient utilization of PI and ultrafast reaction kinetics in aqueous ADIBs are achieved. Consequently, a novel green organic aqueous ADIB based on the flexible PI/NDC/CNT anode and PANI/CNF cathode delivers high specific energy density of 114.3 W h kg^{-1} and high power density of 18.6 kW kg^{-1}. Therefore, the reasonable construction

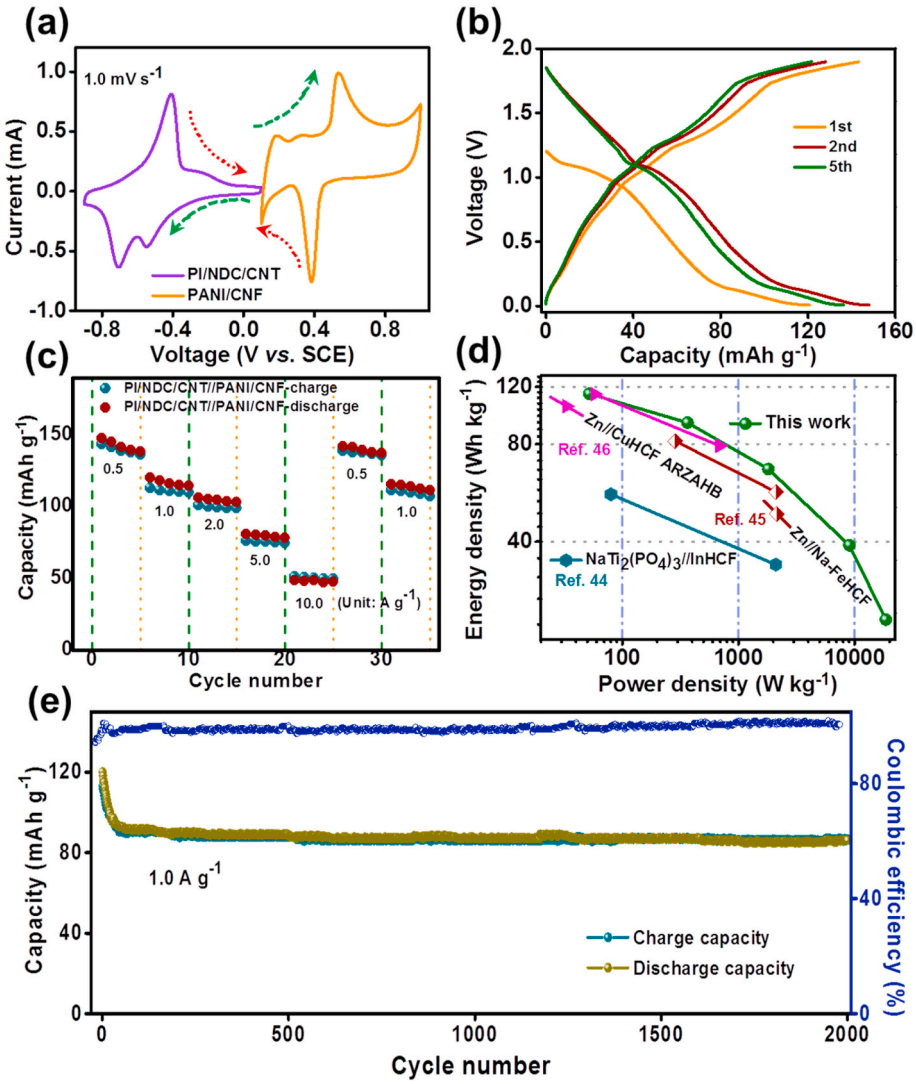

Fig. 6. (a) CV curves of PI/NDC/CNT anode and PANI/CNF cathode, respectively. (b) Charge/discharge voltage profiles at a current density of 0.5 A g^{-1}, (c) rate performance, (d) Ragone plots of our work compared to other previously reported aqueous batteries [44–46], and (e) cycling stability at a current density of 1.0 A g^{-1} of the PI/NDC/CNT//PANI/CNF ADIB.

of electroactive polyimide-based composite electrode can provide new opportunities for development of sustainable and advanced ADIBs.

CRediT authorship contribution statement

Gangyong Zhou: Conceptualization, Methodology, Investigation, Formal analysis, Data curation, Visualization, Writing - original draft, Writing - review & editing. **Xingyu An:** Investigation. **Chunyang Zhou:** Investigation. **Yue Wu:** Investigation. **Yue-E Miao:** Writing - review & editing, Supervision, Funding acquisition. **Tianxi Liu:** Writing - review & editing, Supervision, Funding acquisition.

Declaration of competing interest

The authors declare that they have no known competing financial interests or personal relationships that could have appeared to influence the work reported in this paper.

Acknowledgements

The authors are grateful for the financial support from the Natural Science Foundation of Shanghai (18ZR1401600), the Shanghai Scientific and Technological Innovation Project (18JC1410600), and the Fundamental Research Funds for the Central Universities and Graduate Student Innovation Fund of Donghua University (CUSF-DH-D-2019006).

Appendix A. Supplementary data

Supplementary data to this article can be found online at https://doi.org/10.1016/j.coco.2020.100519.

References

[1] X.L. Dong, L. Chen, J.Y. Liu, S. Haller, Y.G. Wang, Y.Y. Xia, Environmentally-friendly aqueous Li (or Na)-ion battery with fast electrode kinetics and super-long life, Sci. Adv. 2 (2016) 1501038.
[2] Z.W. Guo, Y.Y. Ma, X.L. Dong, J.H. Huang, Y.G. Wang, Y.Y. Xia, Environment-friendly and flexible aqueous zinc battery using an organic cathode, Angew. Chem. Int. Ed. 57 (2018) 11737–11741.
[3] X.F. Wang, Y.M. Qian, L.N. Wang, H. Yang, H.L. Li, Y. Zhao, T.X. Liu, Sulfurized polyacrylonitrile cathodes with high compatibility in both ether and carbonate electrolytes for ultrastable lithium–sulfur batteries, Adv. Funct. Mater. 29 (2019) 1902929.
[4] M. Ma, Y. Yao, Y. Wu, Y. Yu, Progress and prospects of transition metal sulfides for sodium storage, Adv. Fiber Mater. (2020), https://doi.org/10.1007/s42765-020-00052-w.

[5] W. Fan, X. Zhang, C. Li, Functional fibrous compositions: applications and perspectives, Compos. Commun. 15 (2019) 68–75.
[6] M.K. Liu, P. Zhang, Z. Qu, Y. Yan, C. Lai, T.X. Liu, S.Q. Zhang, Conductive carbon nanofiber interpenetrated graphene architecture for ultra-stable sodium ion battery, Nat. Commun. 10 (2019) 3917.
[7] S. Li, Z. Cui, D. Li, G. Yue, J. Liu, H. Ding, S. Gao, Y. Zhao, N. Wang, Y. Zhao, Hierarchically structured electrospinning nanofibers for catalysis and energy storage, Compos. Commun. 13 (2019) 1–11.
[8] J.H. Huang, Z.W. Guo, Y.Y. Ma, D. Bin, Y.G. Wang, Y.Y. Xia, Recent progress of rechargeable batteries using mild aqueous electrolytes, Small Methods 3 (2019) 1800272.
[9] M. Huang, M. Li, C. Niu, Q. Li, L. Mai, Recent advances in rational electrode designs for high-performance alkaline rechargeable batteries, Adv. Funct. Mater. 29 (2019) 1807847.
[10] R. Zhao, X. Lu, C. Wang, Electrospinning based all-nano composite materials: recent achievements and perspectives, Compos. Commun. 10 (2018) 140–150.
[11] H. Li, L. Xu, H. Sitinamaluwa, K. Wasalathilake, C. Yan, Coating Fe_2O_3 with graphene oxide for high-performance sodium-ion battery anode, Compos. Commun. 1 (2016) 48–53.
[12] C. Li, J. Wu, F. Ma, Y. Chen, L. Fu, Y. Zhu, Y. Zhang, P. Wang, Y. Wu, W. Huang, High-rate and high-voltage aqueous rechargeable zinc ammonium hybrid battery from selective cation intercalation cathode, ACS Appl. Energy Mater. 2 (2019) 6984–6989.
[13] Z. Guo, L. Chen, Y. Wang, C. Wang, Y. Xia, Aqueous lithium-ion batteries using polyimide-activated carbon composites anode and spinel $LiMn_2O_4$ cathode, ACS Sustain. Chem. Eng. 5 (2017) 1503–1508.
[14] L. Zhong, Y. Lu, H. Li, Z. Tao, J. Chen, High-performance aqueous sodium-ion batteries with hydrogel electrolyte and alloxazine/CMK-3 anode, ACS Sustain. Chem. Eng. 6 (2018) 7761–7768.
[15] H. Long, W. Zeng, H. Wang, M. Qian, Y. Liang, Z. Wang, Self-assembled biomolecular 1D nanostructures for aqueous sodium-ion battery, Adv. Sci. 5 (2018) 1700634.
[16] C. Liu, X. Chi, Q. Han, Y. Liu, A high energy density aqueous battery achieved by dual dissolution/deposition reactions separated in acid-alkaline electrolyte, Adv. Energy Mater. 10 (2020) 1903589.
[17] R. Chua, Y. Cai, Z.K. Kou, R. Satish, H. Ren, J.J. Chan, L. Zhang, S.A. Morris, J. Bai, M. Srinivasan, 1.3 V superwide potential window sponsored by Na-Mn-O plates as cathodes towards aqueous rechargeable sodium-ion batteries, Chem. Eng. J. 370 (2019) 742–748.
[18] W.J. Song, J. Park, D.H. Kim, S. Bae, M.J. Kwak, M. Shin, S. Kim, S. Choi, J.H. Jang, T.J. Shin, S.Y. Kim, K. Seo, S. Park, Jaboticaba-inspired hybrid carbon filler/polymer electrode for use in highly stretchable aqueous Li-ion batteries, Adv. Energy Mater. 8 (2018) 1702478.
[19] F. Wang, O. Borodin, M.S. Ding, M. Gobet, J. Vatamanu, X. Fan, T. Gao, N. Eidson, Y. Liang, W. Sun, S. Greenbaum, K. Xu, C. Wang, Hybrid aqueous/non-aqueous electrolyte for safe and high-energy Li-ion batteries, Joule 2 (2018) 927–937.
[20] B. He, P. Man, Q. Zhang, H. Fu, Z. Zhou, C. Li, Q. Li, L. Wei, Y. Yao, All binder-free electrodes for high-performance wearable aqueous rechargeable sodium-ion batteries, Nano-Micro Lett. 11 (2019) 101–113.
[21] M. Xia, X. Zhang, T. Liu, H. Yu, S. Chen, N. Peng, R. Zheng, J. Zhang, J. Shu, Commercially available Prussian blue get energetic in aqueous K-ion batteries, Chem. Eng. J. 394 (2020) 124923.
[22] R. Yuksel, O. Buyukcakir, W.K. Seong, R.S. Ruoff, Metal-organic framework integrated anodes for aqueous zinc-ion batteries, Adv. Energy Mater. 10 (2020) 1904215.
[23] D. Bin, W. Huo, Y. Yuan, J. Huang, Y. Liu, Y. Zhang, F. Dong, Y. Wang, Y. Xia, Organic-inorganic-induced polymer intercalation into layered composites for aqueous zinc-ion battery, Inside Chem. 6 (2020) 968–984.
[24] K.W. Nam, H. Kim, Y. Beldjoudi, T.W. Kwon, D.J. Kim, J.F. Stoddart, Redox-active phenanthrenequinone triangles in aqueous rechargeable zinc batteries, J. Am. Chem. Soc. 142 (2020) 2541–2548.
[25] A. Zhou, L. Jiang, J. Yue, Y. Tong, Q. Zhang, Z. Lin, B. Liu, C. Wu, L. Suo, Y.S. Hu, H. Li, L. Chen, Water-in-Salt electrolyte promotes high-capacity $FeFe(CN)_6$ cathode for aqueous Al-ion battery, ACS Appl. Mater. Interfaces 11 (2019) 41356–41362.
[26] H. Pan, K.S. Han, V. Murugesan, J. Xiao, R. Cao, J. Chen, J. Zhang, K.T. Mueller, Y. Shao, J. Liu, Ammonium additives to dissolve lithium sulfide through hydrogen binding for high-energy lithium-sulfur batteries, ACS Appl. Mater. Interfaces 9 (2017) 4290–4295.
[27] H. Jiang, Z. Wei, L. Ma, Y. Yuan, Jessica J. Hong, X. Wu, Daniel P. Leonard, J. Holoubek, J.J. Razink, W.F. Stickle, F. Du, T. Wu, J. Lu, X.L. Ji, An aqueous dual-ion battery cathode of Mn_3O_4 via reversible insertion of nitrate, Angew. Chem. Int. Ed. 58 (2019) 5286–5291.
[28] Q. Nian, S. Liu, J. Liu, Q. Zhang, J. Shi, C. Liu, R. Wang, Z. Tao, J. Chen, All-climate aqueous dual-ion hybrid battery with ultrahigh rate and ultralong life performance, ACS Appl. Energy Mater. 2 (2019) 4370–4378.
[29] M. Wang, Y. Tang, A review on the features and progress of dual-ion batteries, Adv. Energy Mater. 8 (2018) 1703320.
[30] Y. Tao, C. Ding, D. Tan, F. Yu, F. Wang, Aqueous dual-ion battery based on a hematite anode with exposed {1 0 4} facets, ChemSusChem 11 (2018) 4269–4274.
[31] Z. Zhang, X. Hu, Y. Zhou, S. Wang, L. Yao, H. Pan, C.Y. Su, F. Chen, X. Hou, Aqueous rechargeable dual-ion battery based on fluoride ion and sodium ion electrochemistry, J. Mater. Chem. 6 (2018) 8244–8250.
[32] H. Glatz, E. Lizundia, F. Pacifico, D. Kundu, An organic cathode based dual-ion aqueous zinc battery enabled by a cellulose membrane, ACS Appl. Energy Mater. 2 (2019) 1288–1294.
[33] Y. Zhang, Y. An, B. Yin, J. Jiang, S. Dong, H. Dou, X. Zhang, A novel aqueous ammonium dual-ion battery based on organic polymers, J. Mater. Chem. 7 (2019) 11314–11320.
[34] G. Zhou, Y.E. Miao, Z. Wei, L. Mo, F. Lai, Y. Wu, J. Ma, T. Liu, Bioinspired micro/nanofluidic ion transport channels for organic cathodes in high-rate and ultrastable lithium/sodium-ion batteries, Adv. Funct. Mater. 28 (2018) 1804629.
[35] Y. Xu, Y. Zheng, C. Wang, Q. Chen, An all-organic aqueous battery powered by adsorbed quinone, ACS Appl. Mater. Interfaces 11 (2019) 23222–23228.
[36] X. Dong, H. Yu, Y. Ma, J.L. Bao, D.G. Truhlar, Y. Wang, Y. Xia, All-organic rechargeable battery with reversibility supported by "Water-in-Salt" electrolyte, chem, Eur. J. 23 (2017) 2560–2565.
[37] J. Huang, X. Dong, Z. Guo, Y. Wang, Progress of organic electrodes in aqueous electrolyte for energy storage and conversion, Angew. Chem. Int. Ed. 59 (2020) 2–14.
[38] X. Wu, Y. Xu, H. Jiang, Z. Wei, J.J. Hong, A.S. Hernandez, F. Du, X. Ji, NH_4^+ topotactic insertion in berlin green: an exceptionally long-cycling cathode in aqueous ammonium-ion batteries, ACS Appl. Energy Mater. 1 (2018) 3077–3083.
[39] C. Li, W. Yan, S. Liang, P. Wang, J. Wang, L. Fu, Y. Zhu, Y. Chen, Y. Wu, W. Huang, Achieving a high-performance Prussian blue analogue cathode with an ultra-stable redox reaction for ammonium ion storage, Nanoscale Horiz 4 (2019) 991–998.
[40] J. Liu, A.G. Rinzler, H. Dai, J.H. Hafner, R.K. Bradley, P.J. Boul, A. Lu, T. Iverson, K. Shelimov, C.B. Huffman, Fullerene pipes, Science 280 (1998) 1253–1256.
[41] Z. Zhou, C. Lai, L. Zhang, Y. Qian, H. Hou, D.H. Reneker, H. Fong, Development of carbon nanofibers from aligned electrospun polyacrylonitrile nanofiber bundles and characterization of their microstructural, electrical, and mechanical properties, Polymer 50 (2009) 2999–3006.
[42] Z. Ba, Z. Wang, M. Luo, H.B. Li, Y. Li, T. Huang, J. Dong, Q. Zhang, X. Zhao, Benzoquinone-based polyimide derivatives as high-capacity and stable organic cathodes for lithium-ion batteries, ACS Appl. Mater. Interfaces 12 (2019) 807–817.
[43] B. He, P. Man, Q. Zhang, H. Fu, Z. Zhou, C. Li, Q. Li, L. Wei, Y. Yao, All binder-free electrodes for high-performance wearable aqueous rechargeable sodium-ion batteries, Nano-Micro Lett. 11 (2019) 101–113.
[44] L. Chen, H. Shao, X. Zhou, G. Liu, J. Jiang, Z. Liu, Water-mediated cation intercalation of open-framework indium hexacyanoferrate with high voltage and fast kinetics, Nat. Commun. 7 (2016) 11982.
[45] C. Li, D. Zhang, F. Ma, T. Ma, J. Wang, Y. Chen, Y. Zhu, L. Fu, Y. Wu, W. Huang, A high-rate and long-life aqueous rechargeable ammonium zinc hybrid battery, ChemSusChem 12 (2019) 3732–3736.
[46] C. Li, J. Wu, F. Ma, Y. Chen, L. Fu, Y. Zhu, Y. Zhang, P. Wang, Y. Wu, W. Huang, High-rate and high-voltage aqueous rechargeable zinc ammonium hybrid battery from selective cation intercalation cathode, ACS Appl. Energy Mater. 2 (2019) 6984–6989.